Kinetics of the water adsorption driven structural transformation of ZnS nanoparticles

Carmen M. Goodell [1], *Benjamin Gilbert* [2, *], *Steven J. Weigand* [3], *Jillian F. Banfield* [1, 2, *]

[1] Earth and Planetary Science, University of California-Berkeley, Berkeley, CA 94720

[2] Earth Science Division, Lawrence Berkeley National Laboratory, Berkeley, CA 94720

[3] DND-CAT Synchrotron Research Center, Northwestern University, APS/ANL

Argonne, IL 60439

[*] To whom correspondence should be addressed. E-mail: bgilbert@lbl.gov; jbanfield@berkeley.edu

RECEIVED DATE

Abstract

Nanoparticles of certain materials can respond structurally to changes in their surface environments. We have previously shown that methanol, water adsorption, and aggregation-disaggregation can change the structure of 3 nm diameter zinc sulfide (ZnS). However, in prior observations of water-driven structure change, aggregation may also have taken place. Therefore, we investigated the structural consequences of water

adsorption alone on anhydrous nanoparticles that were dried to minimize changes in aggregation. Using simultaneously collected small- and wide-angle x-ray scattering (SAXS/WAXS) data, we show that water vapor adsorption alone drives a structural transformation in ZnS nanoparticles in the temperature range 22 – 40 ˚C. The transition kinetics are strongly temperature dependent, with an activation energy of 58.1 ± 9.8 kJ/mol, consistent with atom displacement rather than bond breaking. At 50 ˚C, aggregate restructuring occurred, increasing the transition kinetics beyond the rate expected for water adsorption alone. The observation of isosbestic points in the WAXS data suggests that the particles do not transform continuously between the initial and final structural state but rather undergo an abrupt change from a less ordered to a more ordered state.

Introduction

Nanoparticles have excess free energy relative to bulk material of the same stoichiometry because a large fraction of their atoms reside at or near the surface. A 3 nm particle of ZnS has approximately half of the total atoms at the particle surface, and these atoms lack a full coordination environment. The excess free energy can cause nanoparticles to seek structures distinct from that of the bulk material and modify nanoparticle phase stability relations (e.g., Ranade et al., (1)). For example, at ambient pressure and temperature, the cubic form of ZnS (sphalerite) is the stable phase in bulk material, yet at small particle size, the hexagonal form (wurtzite) is stabilized (2). Likewise, phase transition pressures can exhibit a size dependence that indicates a surface energy driven modification in phase stability relations. For example, the pressure for the transformation of the wurtzite to NaCl structure of CdSe nanoparticles increases with

decreasing particle size because the surface energy of the cubic phase reduces the stability of the transformation product (3).

Growth and morphology change can reduce the excess surface energy of nanoparticles. Additionally, structural transformation can provide an alternative mechanism for nanoparticles with a metastable structure to reach a lower energy state without accompanying growth. We have observed that a disorder-to-order transformation can be induced by the addition of water to 3 nm ZnS nanoparticles in anhydrous methanol (4). More recently, Bellin *et al*.showed that progressive water adsorption onto γ-Fe_2O_3 nanoparticles causes cell parameter contraction and then relaxation (5). Particle-particle interactions associated with ZnS aggregation can also relieve disorder, a transformation that is reversed by disaggregation (6).

An important challenge for studies that attempt to understand the molecular interactions that drive surface environment driven structural changes within nanoparticles is to separate effects of nanoparticle – nanoparticle from nanoparticle – molecule interactions when both occur simultaneously. To achieve this, we studied the exposure of water vapor to ZnS nanoparticles with an aggregation state that had been previously fixed by rapid drying. We used a combined small- and wide-angle x-ray scattering method to simultaneously monitor the aggregation state and the crystallinity of 3.2 ± 0.7 nm ZnS nanoparticles following the introduction of water vapor. We followed the structural and aggregation states as a function of time and temperature in order to evaluate the role of water adsorption and to estimate the energy of activation of the resulting transformation.

Experimental Methods

Nanoparticle synthesis and handling

3.2 ± 0.7 nm diameter zinc sulfide (ZnS) nanoparticles were synthesized at room temperature in 100 ml anhydrous methanol by adding 5 mL of a saturated methanol solution of sodium sulfide solution dropwise into 2.5 mL of 1 M zinc chloride solution in methanol with rapid stirring. The solution was stirred for fifteen minutes after Na_2S addition was completed and then filtered and rinsed with three times the volume to remove excess Na^+, Cl^-, and S^{2-} ions. The solution was filtered until the aggregated nanoparticles formed a homogenous gel.

The nanoparticle suspension was placed under vacuum (approximately 10^{-4} Torr) at room temperature for several hours to rapidly evaporate the methanol without nanoparticle growth. The dry nanoparticles were brought back to atmospheric pressure with argon gas to avoid exposure to moisture in air. The drying process partially collapsed the gel, producing macroscopic aggregates that were ground to a fine powder that was stored in argon until needed for experimentation. Previous characterization of material prepared with this approach showed that the dried aggregates retained an open, fractal geometry and the structure of the nanoparticles is indistinguishable from the as-synthesized particles in the original solution (6).

Exposure of nanoparticles to water vapor

Dry ZnS nanoparticles were packed under argon gas into a 1.5 mm diameter special glass capillary (Charles Supper, MA), which had previously been shortened and flamed sealed on one end. Particles were held in place by a small dry cotton plug. The capillary was inverted (so that the nanoparticles were at the top of the capillary), a second

cotton plug, which had been soaked in water, inserted into the capillary, and the capillary sealed (Figure 1). Care was taken to prevent direct contact between the nanoparticle powder and liquid water. The capillary was placed in a THMS600 heating stage (Linkam Scientific Instruments) and mounted on the 5-ID-D beamline in the DND-CAT sector of the Advanced Photon Source at Argonne National Laboratory for simultaneous SAXS and WAXS analysis. The transformation was observed at 22, 30, 40 and 50 ˚C.

Synchrotron x-ray experiments

Experiments were conducted at the Advanced Photon Source at Sector 5 (DuPont-Northwestern-Dow—Collaborative Access Team) in the ID-D hutch. The hutch was set up for simultaneous collection of both small-angle x-ray scattering (SAXS) and wide-angle x-ray scattering (WAXS) by two 2D detectors. These were a MarCCD 165 detector (Mar USA) for SAXS, and a specially built phosphor/fiber optic taper coupled CCD detector from Roper Scientific (WAXS). The capillary was centered both vertically and horizontally relative to the 1 x 1 mm x-ray beam spot before data acquisition. Aluminum sheets were used to attenuate the WAXS signal relative to the SAXS signal to ensure that both detectors stayed within their dynamic range. The heating stage has an accuracy of 0.75 °C and complete heating of the stage and the sample took less than 5 minutes.

X-ray scattering data were collected for 45-60 seconds (depending on the sample scattering strength) using a wavelength of 0.8265 Å. For each time point, 6 scans were taken in rapid succession plus six dark scans to allow algorithmic removal of spurious intensity spots associated with random cosmic radiation (zingers). Data processing was performed using FIT2D (7). Specifically, each image was corrected for detector dark current, non-uniformity, and distortion then normalized to the incident flux. The exposures were averaged together and integrated over a full circle for the SAXS camera

and a half circle for the WAXS camera using FIT2D to generate two-column files of scattering intensity versus 2θ (7).

Wide-angle x-ray scattering data analysis

The WAXS data were processed using routines written in the IGOR-PRO analysis software. The nanoparticle structure transformation was followed by fitting Voigt profiles to the cubic ZnS Bragg peaks, which narrowed following water adsorption. In order to quantify the transformation kinetics, we report peak width of the (311) reflection plotted for each time point. The resulting curves of peak width vs. time were fit using a rate equation discussed below. All scans from all temperatures were analyzed over the same scattering angle that encompassed both the (220) and (311) reflections. In a separate data treatment, the WAXS patterns were normalized with respect to integrated scattering intensity over the full range of scattering angles.

Small-angle x-ray scattering data analysis

Small angle x-ray scattering is analogous to wide-angle x-ray scattering but probes longer length scales. Because nanoparticle aggregates generally do not exhibit long-range periodicity, the SAXS patterns do not show sharp scattering features. Nevertheless, quantitative simulation and analysis of SAXS data can be performed if assumptions are made about the size and size distribution of the primary particles and the way that they are distributed in space (8). The initial material, and the 22 - 40 ˚C studies gave SAXS patterns typical of fractal aggregates (9). The high temperature data are unusual in that they exhibit an evolution between two distinct types of scattering, and thus are very difficult to interpret using existing models that assume any single type of aggregate morphology (10). Specifically, at the highest temperature, the SAXS pattern

evolved to display features typical of more compact nanoporous granular media (11)(12), in which the fractal structure was lost at short range. There are no robust methods for analysis of this type of SAXS data. Therefore, the evolution of the high-*q* region was analyzed by a maximum entropy model (MEM) that derived a particle size distribution from the data (assuming spherical nanoparticles), but making no assumptions about the particle arrangement (13). Thus, the trends in medium- and long-range aggregate structure are discussed qualitatively, while only short-range changes in apparent nanoparticle size and size distribution are analyzed quantitatively via the MEM.

Transmission electron microscopy

The transformed material was characterized by transmission electron microscope (TEM) imaging and electron diffraction. In an experiment analogous to the synchrotron high temperature experiment, dried nanoparticles were placed in an oven that had been equilibrated with a dish of water at 50 °C for 18 hours. Particles suspended in water were dried onto a formvar-coated copper grid and examined in a JEOL JEM 2011 TEM at 200 keV and magnifications from 200K to 600K times.

Results

WAXS data show that dried anhydrous ZnS nanoparticles undergo a structural transformation when exposed to water vapor over a temperature range of 22–50 °C (Figure 2). Diffraction patterns taken prior to water exposure are similar to the patterns previously observed from ZnS nanoparticles synthesized with the same method but analyzed in methanol (4). In each case, the diffraction patterns indicate the presence of nanoscale sphalerite particles. However, the diffraction data acquired immediately prior

to vapor exposure show evidence of more crystallinity than previously observed for samples analyzed in methanol (Figure 2c), probably because of adsorption of atmospheric water vapor during transport and handling.

Figure 2 shows an example fit to the WAXS data. In addition to the sphalerite components, one additional broad Gaussian peak was necessary to account for background scattering beneath the 220 and 311 peaks. This peak diminishes in areas with increasing reaction time and could not be attributed to wurtzite. Thus, we infer the presence of a highly disordered fraction. In order to quantify the kinetics of the structural transformation, peak position, width and intensity of the (220) and (311) peaks for each data curve were fitted. The (220) and (311) peaks were chosen for kinetic analysis to avoid complications arising from the overlap of the (111) and (200) peaks. The peak intensity was the only parameter of the disordered component that was allowed to vary.

The SAXS data taken simultaneously with the WAXS patterns exhibit small time-dependent trends for the low temperature experiments ($20 - 40$ ˚C; Figure 3a). In contrast, the SAXS data acquired for the highest temperature studied (50 ˚C) displayed a marked evolution. The SAXS profiles can be interpreted in terms of aggregate type by analogy with published results from colloidal aggregates (9)(10)(12). The initial and subsequent low temperature SAXS data are typical of small-angle scattering from fractal aggregates with a primary particle size of 3-4 nm. During these experiments, there is a small shift in the high-q data that is consistent with an increase in the primary particle size. However, this phenomenon could be caused either by nanoparticle growth or by an increase in the apparent particle size due to the adsorption of multiple water layers on the nanoparticle surfaces.

At high temperature, the SAXS profile is modified profoundly, indicating that the morphology changes with time from a statistically fractal aggregate into a nanoporous granular aggregate (i.e., tightly-packed nanoparticle assemblies). The SAXS pattern from porous grains is very distinct, possessing two Porod regions (in which the intensity, $I(q) \propto q^4$) that are associated with scattering from the surfaces of the granular aggregates and the surfaces of the nanoparticles (12). However, because the slope of the low-q region reaches a maximum of –3.3 rather than –4, the data reveal that the fractal aggregates do not fully transform into granular aggregates over the time course of the experiment.

The lack of methods for the analysis of the high temperature data necessitated the use of a model-free approach that could be used to obtain information about both the low- and high-temperature data. We employed the maximum entropy method (13) to generate size distribution histograms of populations of scattering objects that are consistent with the SAXS data. Figure 3 presents the results for the 22 ˚C data.

Discussion

1) Interpreting WAXS data: coarsening versus crystallization

There are several plausible interpretations of the WAXS data. X-ray diffraction peaks may be broadened both by small particle size and by the presence of structural disorder. Hence the observed peak sharpening may be caused either by nanoparticle growth or by increasing crystallinity. While it is frequently possible to resolve size and strain contributions to peak broadening by analyzing the diffraction data (14), such an analysis is impossible in this system because too few peaks are resolved.

We have shown previously that the observed transformation is described by a strong reduction in structural disorder rather than an increase in nanoparticle size (4)(15). When water was added to ZnS nanoparticles in anhydrous methanol, measurements of the semiconductor band gap by UV-vis absorption spectroscopy showed that nanoparticle growth did not occur over 24 hours at room temperature. Nanoparticle growth would diminish the quantum confinement effect and reduce the band gap, but this was not observed. In the absence of a solvent, dissolution-reprecipitation based growth is impossible, and dry nanoparticles can grow only via sintering. While it was not possible to recover and image the nanoparticle samples studied by SAXS-WAXS, a portion of untransformed material was independently heated in high humidity air (105 mmHg partial pressure of water) at 50 ˚C for 18 hours. TEM imaging of this material is given in Figure 4. These nanoparticles were heat treated for 9 times longer than the experiment at DND-CAT but displayed an average particle size of 3.2 $\pm$ 0.7 nm. This size is consistent with the average initial particle size found by Zhang, Gilbert et al. using the same synthesis method. However, because trends in the low temperature, high-q SAXS data are consistent with slight increases in particle size the simultaneous SAXS/WAXS data must be considered in detail in order to fully exclude the possibility of some crystal growth.

Analysis of the trends in the SAXS data show that the apparent growth at 22 ˚C exhibited a threshold that is not reproduced in the WAXS kinetics data (Fig. 3b and 3c). If particle growth were the sole cause of diffraction peak sharpening, trends in these two data sets should be highly correlated. Moreover, Scherrer analysis of the width of the ZnS (311) peak indicates that a change in particle diameter of more than a nanometer would

be required for consistence with the WAXS results. By contrast, the SAXS data indicate that the mean diameter increases by a maximum of 0.3 nm. Therefore, we interpret the apparent diameter increase as representing the adsorption of water molecules to the surface of the nanoparticles.

2) What drives the transformation? Water binding versus aggregation

Prior and present observations indicate that the more crystalline structure is the stable phase for the ZnS nanoparticles in the presence of surface interactions that include aggregation and the adsorption of water. Heat alone is not sufficient to cause the transformation, as ZnS nanoparticles synthesized and studied in anhydrous methanol showed very little structural change when heated at 60 °C for 16 hours. By contrast, when water is added (10 % v/v), the nanoparticles rapidly transform at 50 °C (Figure 2c).

The simultaneous acquisition of SAXS and WAXS data permitted us to test the premise that water vapor can drive structural change with negligible change of aggregate state. Indeed, there is no evidence of changes in medium- and long-range aggregate morphology in the temperature range 22–40 °C because there is no evolution in the low–q SAXS data for these temperatures.

Previous investigators studied the structural consequences of water adsorption onto initially anhydrous 11 nm γ-Fe_2O_3 particles (5) and found that two regimes of water vapor partial pressures. For $p/p_0 < 0.1$, water bound irreversibly, causing lattice contraction. At higher pressure, layers of liquid-like water developed on the surfaces, reversing the contraction. While the chemical interactions between water and oxide or sulfide surfaces are different, it is reasonable to assume that regimes of strong binding and liquid development exist in the present system. The calculated partial pressures in our lower

temperature experiments (22–40 °C) correspond to the regime of strong binding observed by Belin *et al*, while the humidity during the 50 °C experiments corresponds to the regime in which multiple layers of liquid-like water formed on the surface of the nanoparticles. Thus, we infer that it could be the deposition of liquid water that permits the observed aggregate restructuring. Although it takes approximately 30 minutes for complete adsorption at the partial pressure for 22 °C, the change in nanoparticle structure begins immediately (Figure 3b). The early and continuous structural change suggests that it is the initial adsorption of water to higher energy sites that most significantly decreases surface energy, stabilizing the more crystalline structure and enabling the transformation.

3) ZnS Structures Observed in the Transformation

The reduction of disorder is clearest effect of water binding, but there are additional structural consequences. In a previous study it was found that powder diffraction from ZnS nanoparticles with a nominally cubic structure were not perfectly described by a cubic unit cell, and XRD refinement was possible only when a lower symmetry structure was employed (16). Analyses of the peak positions of the present data likewise reveal that these nanoparticles are not perfectly cubic but approach the cubic sphalerite structure as the transformation proceeds. In a separate analysis, we fitted the WAXS data using a tetragonal space group (*I 4m2*), and observed opposing trends in the (*a,b*) and *c* parameters during this transition, but with the overall unit cell volume conserved.

4) ZnS Structures Observed in the Transformation

Further insight into the transformation is gained by plotting the WAXS data with constant scattering intensity. For all temperatures, the evolving WAXS patterns pass

through points of constant intensity, two for each peak (Figure 5), that we identify as isosbestic points. More commonly found in optical absorption spectra (17), the concepts of isosbestic points in diffraction data has been discussed (18). The observation of isosbestic points has strong implications for the mechanism of transformation. Their presence implies that the nanoparticles transform between two structural states, and that the data do not represent a continuum of structural configurations. Thus, water binding stabilizes the more crystalline phase, but an individual nanoparticle transforms abruptly only when thermal energy allows an activation barrier to be overcome. Rather than changing continuously as water molecules adsorb to the surface of the nanoparticles, the nanoparticles presumably transform randomly once the sufficient water is adsorbed. In this model, it is the activation barrier for the solid-state transformation that causes the variation in transition rate with temperature. This mechanism implies that the transformation kinetics will exhibit an exponential time dependence. Consequently, we fitted the kinetics data with a rate law based on an exponential decay curve of the form $N = N_0 + B\mathrm{e}^{-k(t-t_0)}$, as shown in Figure 6. N_0 and t_0 are time and intensity offsets that were varied freely for each sample. N_o accounted for the practical intervals between the preparation and mounting of each sample.

5) Activation Energy of the Transformation

We used the empirical Arrhenius equation to estimate the energy of activation for the transformation. The dependence of the reaction rate with temperature is

$$k_{obs} = A \cdot e^{\frac{-E_A}{RT}},$$

where k_{obs} is the observed reaction rate obtained from fits to the WAXS kinetics data as described above. A is pre-exponential factor, E_A is the apparent energy of activation, R is

the noble gas constant and T is temperature in Kelvin. A plot of $ln\ k$ versus T^{-1} is given as an inset to Figure 6. The curve is nonlinear when all temperature points are included. However, when the 50 °C data are excluded, the trend for the lower temperature data is linear, as expected for a transformation that proceeds by a single thermally activated pathway. The activation energy for this transformation using the 22–44 °C data is 58.1 $\pm$ 9.8 kJ/mol. The transformation at 50 °C is faster than expected by Arrhenius analysis of the lower temperature data, suggesting an additional transformation mechanism operates higher temperature, most likely an aggregation effect. This magnitude of the activation energy indicates that the process does not involve water dissociation (19) or the breaking of ZnS bonds, but is associated with restructuring (bond bending) within the nanoparticles. If bonds were actually breaking and reforming, we would expect an activation energy on the order of hundreds of kilojoules per mole.

6) Proposed Model of the Transformation

The results and analysis lead to a model of the water vapor driven transformation of 3 nm ZnS particles that is shown graphically in Figure 7. The key points in this model are that water vapor rapidly permeates the loose aggregate of anhydrous nanoparticles, binding to the surfaces strongly but without dissociation. This interaction stabilizes a more crystalline structure, but the transformation proceeds only when thermal energy initiates an abrupt solid-state transformation. It is likely that the transformation is nucleated at the surface of the nanoparticle. At the highest temperature studied, the increased surface coverage of water allows the nanoparticles to rearrange within the aggregate, forming more particle-particle contacts, which are known to increase crystallinity (6). These additional contacts provide an additional mechanism to lower

surface energy and stabilize the more crystalline structure. Consequently, the rate of transformation is faster at this temperature than expected for water binding alone.

Conclusions

Water adsorption and aggregation both drive structural transformation in 3.2_nm ZnS nanoparticles. Observation of the water driven transformation with no change in aggregation state provides insight into molecular interactions with nanoparticle surfaces . Individual nanoparticles do not transform gradually, but switch abruptly from an initial, disordered structure to a final, more crystalline structure. Our work has clarified that both interactions with molecules and with other particles can have profound effects on disorder within nanocrystals.

Acknowledgments

Financial support was provided by the NSF IGERT fellowship; the Director, Office of Science, Office of Basic Energy Sciences, of the U.S. Department of Energy under Contract No. DE-AC02-05CH11231; and from Lawrence Berkeley National Lab. The SAXS/WAXS experiments were performed at the DuPont-Northwestern-Dow Collaborative Access Team (DND-CAT) Synchrotron Research Center at the Advanced Photon Source (APS). DND-CAT is supported by the E.I. DuPont de Nemours & Co., The Dow Chemical Company, the U.S. National Science Foundation through Grant DMR-9304725 and the State of Illinois through the Department of Commerce and the Board of Higher Education Grant IBHE HECA NWU 96. Use of the APS is supported by the U. S. Department of Energy, Office of Science, Office of Basic Energy Sciences, under Contract No. W-31-109-Eng-38.

(1) Ranade, M. R.; Navrotsky, A.; Zhang, H. Z.; Banfield, J. F.; Elder, S. H.; Zaban, A.; Borse, P. H.; Kulkarni, S. K.; Doran, G. S.; Whitfield, H. J. Proc. Natl. Acad. Am. **2002**, 99, 6476.

(2) Zhang, H. Z.; Huang, F.; Gilbert, B.; Banfield, J. F. J. Phys. Chem. B **2003**, 107, 130511.

(3) Tolbert, S. H.; Alivisatos, A. P. *Science* 1994, **265**, 373.

(4) Zhang. H.; Gilbert, B.; Huang, F.; Banfield, J. F. *Nature* 2003, 424, 1025.

(5) Belin. T.; Millot, N.; Villiéras, F.; Bertrand, O.; Bellat, J. P. *J. Phys. Chem. B* 2004, *108,* 5333.

(6) Huang, F.; Gilbert, B.; Zhang, H.; Banfield, J. F. *Phys. Rev. Lett.* **2004**, *92*, 155501.

(7) Hammersley, A.P. *ESRF Internal Report*, **ESRF97HA02T**, "FIT2D: An Introduction and Overview", (1997)

(8) Lindner, P.; Zemb, Th. (Eds.) *Neutron, X-ray and Light Scattering: Introduction to an Investigative Tool for Colloidal and Polymeric Systems*. North-Holland, Amsterdam, (1991).

(9) Bushell, G. C.; Yan, Y. D.; Woodfield, D.; Raper, J.; Amal, R. *Adv. Colloid Interf. Sci.* 2002, 95, 1.

(10) Reidy, R. F.; Allen, A. J.; Krueger, S. *J. Non-Cryst. Solids* 2001, 285, 181.

(11) Allen, A. J.; Krueger, S.; Skandan, G.; Long, G. G.; Hahn, H.; Kerch, H. M.; Parker, J. C.; Ali, M. N. *J. Am. Ceram. Soc. 1996,* **79**, 1201.

(12) Spalla, O.; Lyonnard, S.; Testard, F. *J. Appl. Cryst., 2003,* **36**, 338-347.

(13) Long, G. G.; Krueger, S.; Jemian, P. R.; Blank, D. R.; Burdette, H. E.; J. P., Cline; J. P.; Gerhart, R. A. *J. Appl. Cryst. 1990,* **23**, 535.

(14) Langford, J. I.; Louër, D. *Rep. Prog. Phys.* 1996, 59, 131.

(15) Gilbert, B.; Zhang, H. Z.; Huang, F.; Banfield, J. F.; Ren, Y.; Haskel, D.; Lang, J. C.; Srajer, G.; Jurgensen, A.; Waychunas, G. A. *J. Chem. Phys.* 2004, 210, 11785.

(16) Gilbert, B.; Zhang, H.; Chen, B.; Kuntz, M.; Huang, F.; Banfield, J. F. *Phys. Rev. B* 2006, 74, 115405.

(17) Tratnyek, P. G.; Reilkoff, T. E.; Lemon, A. W.; Scherer, M. M.; Balko, B. A.; Feik, L. M.; Henegar. B. D. *The Chemical Educator* 2001, 6, 172.

(18) Johnson, R. W. *Journal of Non-Crystalline Solids* 1986, 88, 366

(19) Gilbert, B., Huang, F., Lin, Z., Goodell, C.; Zhang, H. Z.; Banfield, J. F. *Nano Lett.* 2006, 6, 605.

Kinetics of the water adsorption driven structural transformation in ZnS nanoparticles

Carmen M. Goodell [1], Benjamin Gilbert [2, *], Steven J. Weigand [3], Jillian F. Banfield [1, 2, *]

FIGURES

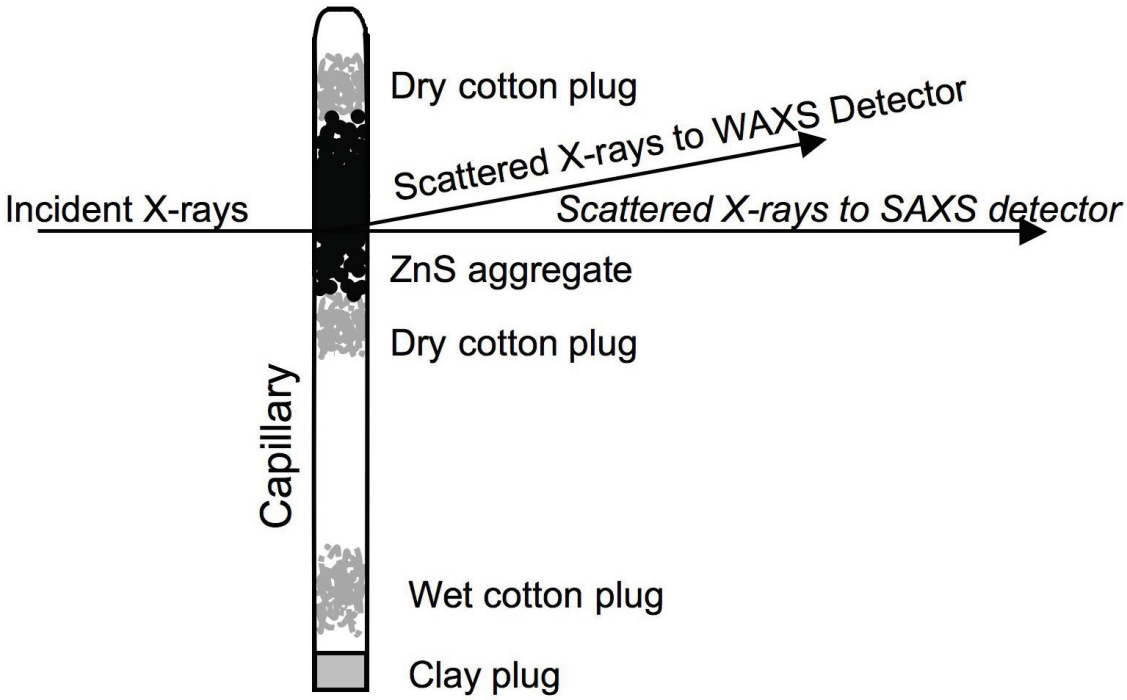

Figure 1 Experimental Setup. A special glass capillary is loaded with the vacuum dried ZnS aggregate sandwiched between two small amounts of dry cotton. A third piece of cotton that has been saturated with water is placed at the bottom of the capillary, without wetting the dry cotton plug and sample. The capillary is sealed with clay and epoxy to prevent evaporation of the water. Incident x-rays (λ=0.82656 Å) are transmitted through the sample, and small-angle scattering and wide-angle scattering are collected simultaneously.

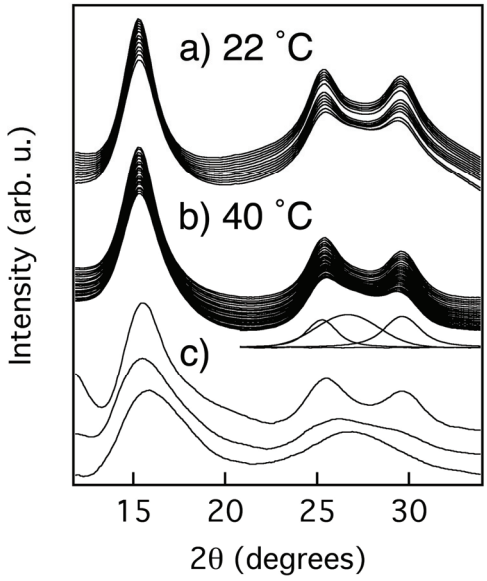

Figure 2 (a) and (b) Wide-angle x-ray scattering (WAXS) observations of the transformation at two temperatures. Following exposure to water vapor, the particles become more crystalline, as seen by the diffraction peak sharpening. These data were collected at 22 °C over 130 minutes (b) and 40 °C over 75 minutes (a) at beamline 5-ID-D at the Advanced Photon Source. Transformation progress was quantified with fits to the sphalerite (220) and (311) peaks, as described in the text, and best-fit components are given beneath one curve. For comparison, (c) shows (bottom to top) WAXS data from as-synthesized nanoparticles in methanol, the same nanoparticles heated at 60 ˚C for 18 hours without water addition, and nanoparticles heated at 60 ˚C following water addition. Minimal structure modification is observed in the absence of water.

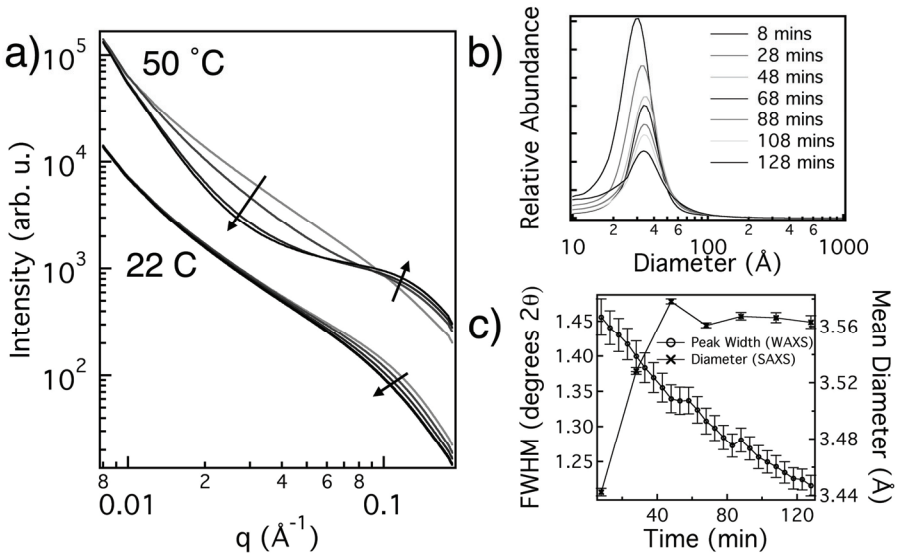

Figure 3 (a) Small-angle x-ray scattering (SAXS) observations of changes in aggregate morphology (low-*q* region) and the apparent nanoparticle size (high-*q* region) following exposure to water vapor. Arrows indicate the direction of lineshape trends with time. At lower temperatures, an apparent increase in particle size is observed but without change in aggregate morphology. By contrast, the 50 ˚C data indicate significant aggregate restructuring occurs. (b) Plot of the evolution in apparent particle size at 22 ˚C determined by maximum entropy method analysis (c) Comparison of the time dependence of the SAXS and WAXS data at 22 ˚C.

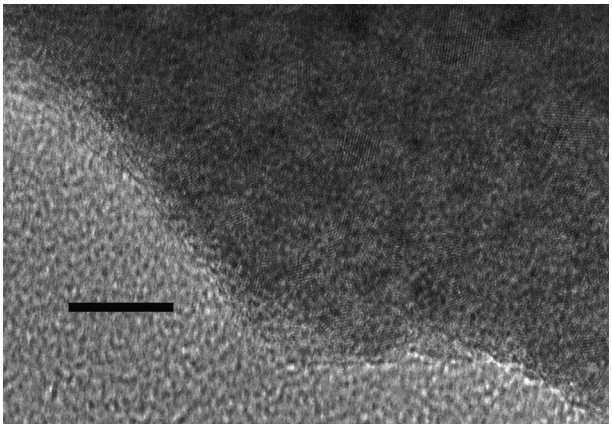

Figure 4 Transmission electron micrograph of an aggregate of ZnS nanoparticles. While individual nanoparticles are not found, the high-resolution imaging is consistent with a mean diameter of 3 - 4 nm, the same as for the as-synthesized material. These particles have been vacuum dried and placed in an oven with water vapor at 50 °C for 18 hours. Scale bar =10 nm.

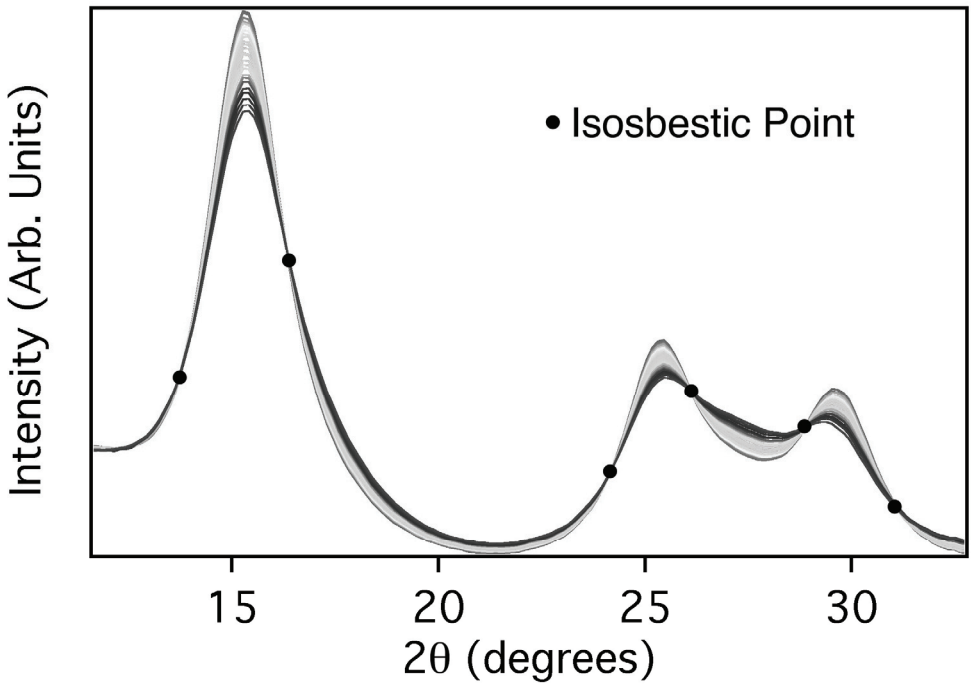

Figure 5 40 ˚C WAXS data normalized with respect to total scattering intensity. The presence of conserved crossover (isosbestic) points indicates an abrupt transition between two structural states, rather than a gradual lessening of strain and disorder.

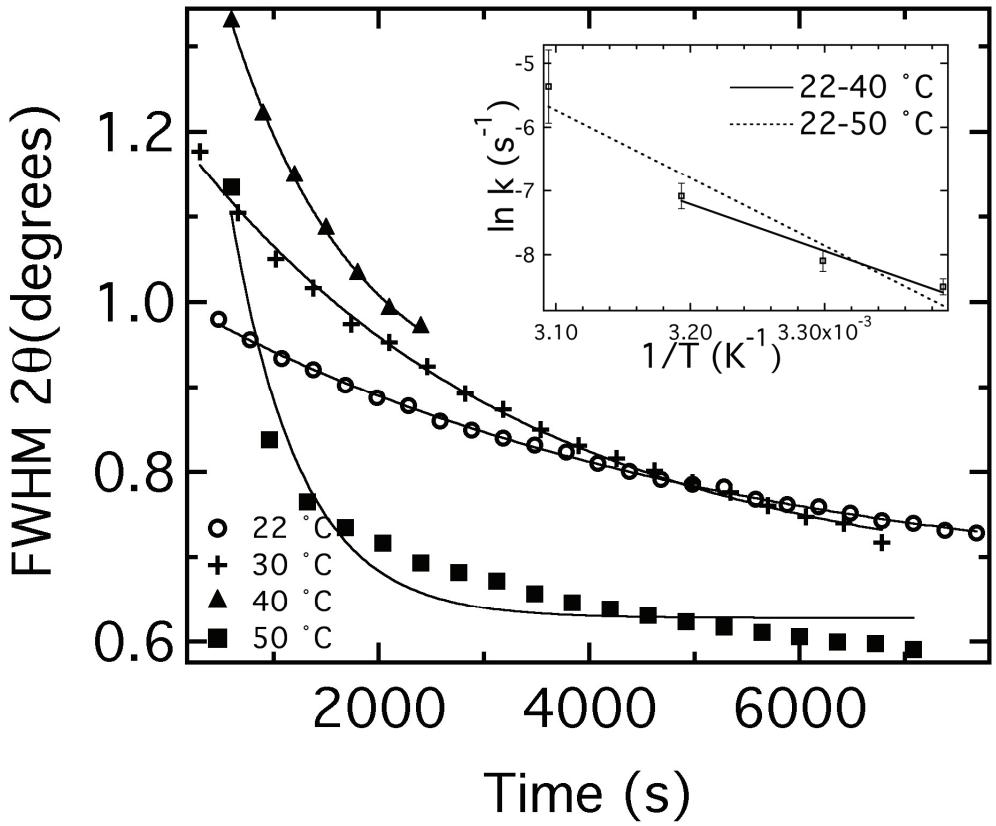

Figure 6 The peak width, 2θ (degrees), of the (311) peak is extracted from each spectrum in WAXS data and plotted against time. The kinetics curves for 22 – 40 °C experiments are well fit using a simple exponential decay curve. The 50 °C data are not fit as well with this approach, suggesting an additional transformation pathway at high temperature. Inset: The Arrenhius plot of the rate coefficients shows the lower temperature data (solid line) lie on a line corresponding to an activation energy of 53.1 kJ mol^{-1}. The dashed line shows the Arrhenius fit to all temperatures.

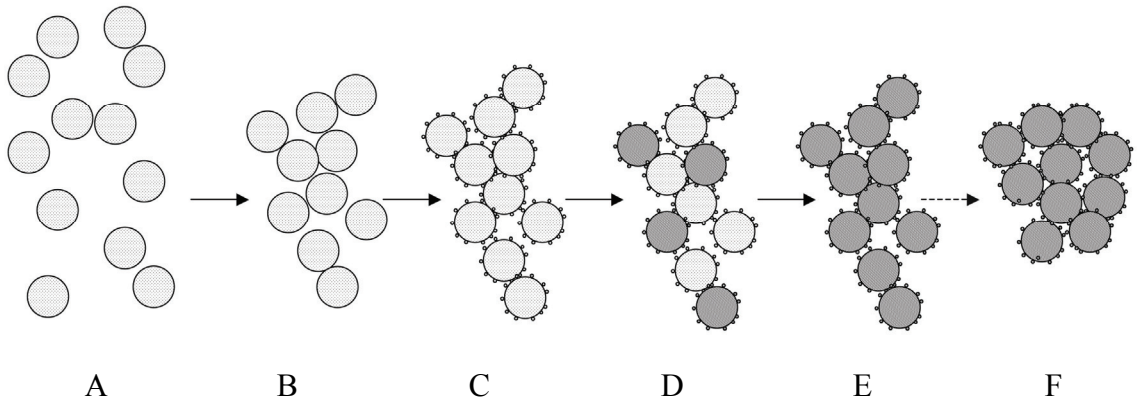

Figure 7 The proposed model for the water vapor driven transformation. A. As-synthesized nanoparticles in methanol form an extended gel-like network. B. When the nanoparticles are rapidly vacuum-dried, particle-particle contacts are formed at random, creating a fractal aggregate. C. When water vapor is introduced, it is rapidly adsorbed on the nanoparticle surfaces throughout the aggregate, and stabilizes a more crystalline structure D. Individual nanoparticles undergo abrupt, random, thermally-activated transformations to the more crystalline structure (dark gray circles). E. Eventually, all the particles have transformed to the more ordered structure. F. At high temperature (50 °C), increased surface coverage of water allows the particles to rearrange the aggregate, forming more particle-particle contacts and more ordered void space within the aggregate. Additional particle-particle interactions increase the transformation rate.